emeraldinsight

Rapid Prototyping Journal

Robocasting of carbon-alumina core-shell composites using co-extrusion
Zongwen Fu, Matthias Freihart, Tobias Schlordt, Tobias Fey, Torsten Kraft, Peter Greil, Nahum Travitzky,

Article information:

To cite this document:
Zongwen Fu, Matthias Freihart, Tobias Schlordt, Tobias Fey, Torsten Kraft, Peter Greil, Nahum Travitzky, (2017) "Robocasting of carbon-alumina core-shell composites using co-extrusion", Rapid Prototyping Journal, Vol. 23 Issue: 2, pp.423-433, https://doi.org/10.1108/RPJ-12-2015-0191
Permanent link to this document:
https://doi.org/10.1108/RPJ-12-2015-0191

Downloaded on: 10 June 2018, At: 09:18 (PT)
References: this document contains references to 47 other documents.
To copy this document: permissions@emeraldinsight.com
The fulltext of this document has been downloaded 348 times since 2017*

Users who downloaded this article also downloaded:

(2017),"Direct-print photopolymerization for 3D printing", Rapid Prototyping Journal, Vol. 23 Iss 2 pp. 337-343 https://doi.org/10.1108/RPJ-11-2015-0172

(2017),"Direct selective laser sintering and melting of ceramics: a review", Rapid Prototyping Journal, Vol. 23 Iss 3 pp. 611-623 https://doi.org/10.1108/RPJ-11-2015-0178

Access to this document was granted through an Emerald subscription provided by emerald-srm:161385 []

For Authors

If you would like to write for this, or any other Emerald publication, then please use our Emerald for Authors service information about how to choose which publication to write for and submission guidelines are available for all. Please visit www.emeraldinsight.com/authors for more information.

About Emerald www.emeraldinsight.com

Emerald is a global publisher linking research and practice to the benefit of society. The company manages a portfolio of more than 290 journals and over 2,350 books and book series volumes, as well as providing an extensive range of online products and additional customer resources and services.

Emerald is both COUNTER 4 and TRANSFER compliant. The organization is a partner of the Committee on Publication Ethics (COPE) and also works with Portico and the LOCKSS initiative for digital archive preservation.

*Related content and download information correct at time of download.

Downloaded by FRIEDRICH ALEXANDER UNIVERSITAET ERLANGEN NUERNBERG At 09:18 10 June 2018 (PT)

Robocasting of carbon-alumina core-shell composites using co-extrusion

Zongwen Fu, Matthias Freihart, Tobias Schlordt and Tobias Fey
Department of Materials Science, Glass and Ceramics, Friedrich-Alexander University Erlangen-Nürnberg, Erlangen, Germany
Torsten Kraft
Mechanics of Materials IWM, Fraunhofer Institute, Freiburg, Germany, and
Peter Greil and Nahum Travitzky
Department of Materials Science, Glass and Ceramics, Friedrich-Alexander University Erlangen-Nürnberg, Erlangen, Germany

Downloaded by FRIEDRICH ALEXANDER UNIVERSITAET ERLANGEN NUERNBERG At 09:18 10 June 2018 (PT)

Abstract

Purpose – This study aims to achieve the fabrication of three-dimensional core-shell filament-based lattice structures by means of robocasting combined with co-extrusion. For core and shell materials, colloidal gels composed of submicron carbon and alumina powders were developed, respectively. Simultaneously, the co-extrusion process was also studied by numerical simulation to investigate the feed pressure-dependent wall thickness.

Design/methodology/approach – Significant differences in the rheological behavior of the carbon and alumina gels were observed because of differences of the particle morphology and surface chemistry of the carbon and alumina powders. Precise control over the cross-sectional diameter of the core and shell green state elements was achieved by alteration of the feed pressures used during co-extrusion.

Findings – After subsequent thermal treatment in an oxidizing atmosphere (e.g. air), in which the carbon core was oxidized and burned out, lattice structures formed of hollow filaments of predetermined wall thickness were manufactured; additionally, C-Al_2O_3 core-shell filament lattice structures could be derived after firing in an argon atmosphere.

Originality/value – Green lattice truss structures with carbon core and alumina shell filaments were successfully manufactured by robotically controlled co-extrusion. As feedstocks carbon and alumina gels with significantly different rheological properties were prepared. During co-extrusion, the core paste exhibited a much higher viscosity than the shell paste, which benefited the co-extrusion process. Simultaneously, the core and shell diameters were exactly controlled by core and shell feed pressures and studied by numerical simulation. The experimentally and numerically derived filament wall thickness showed qualitative agreement with each other; with decreasing core pressure during co-extrusion, the wall thickness increased.

Keywords Additive manufacturing, CFD simulation, Co-extrusion, Colloidal gel, Hollow ligament, Robocasting

Paper type Research paper

1. Introduction

Robocasting is a manufacturing process to fabricate filament-based complex structures which have a wide applicability, in areas such as catalyst support, implantable biomaterials (e.g. bone and dental prostheses) and ceramic filters for molten metals (de Hazan *et al.*, 2012; He *et al.*, 2008; Lewis, 2006; Lewis *et al.*, 2006). In comparison to other shaping techniques, such as three-dimensional (3D) printing (Fu *et al.*, 2013) and fused deposition modelling (FDM) (Roberson *et al.*, 2015), robocasting enables a robotically controlled extrusion of a continuous rod-like filament through a nozzle with defined shape and diameter to build complex 3D ceramic structures with high construction velocity and variable filament diameter at room temperature (Travitzky *et al.*, 2014). In this technique, binder-assisted aqueous colloidal gels with high solid loading of ceramic particles are used as a casting feedstock for manufacturing the 3D lattice structures with free spanning ligaments (Cesarano *et al.*, 1998; Schlordt *et al.*, 2012). A variety of casting gels composed of ceramic (Lewis, 2006; Lewis *et al.*, 2006; Mason *et al.*, 2009; Miranda *et al.*, 2006; Morissette *et al.*, 2000; Nadkarni and Smay, 2006; Saiz *et al.*, 2007; Şakar-Deliormanlı *et al.*, 2008; San Marchi *et al.*, 2003; Schlordt *et al.*, 2012; Smay *et al.*, 2002, 2004; Stuecker *et al.*, 2003; Wang and Shaw, 2005), glass (Doiphode *et al.*, 2011), polymer (Gratson *et al.*, 2004; Lorang *et al.*, 2011; Xie *et al.*, 2006) and metal (Ahn *et al.*, 2011; Li *et al.*, 2010; Michielsen *et al.*, 2013) fillers have previously been developed and optimized for robocasting. Furthermore, filaments with different cross-sectional geometries, e.g. circular, quadratic, hexagonal and even

The current issue and full text archive of this journal is available on Emerald Insight at: **www.emeraldinsight.com/1355-2546.htm**

Rapid Prototyping Journal
23/2 (2017) 423–433
© Emerald Publishing Limited [ISSN 1355-2546]
[DOI 10.1108/RPJ-12-2015-0191]

The authors would like to acknowledge the financial support from the Deutsche Forschungsgemeinschaft (DFG TR 250/6-1) and the Exzellenzcluster "Engineering of Advanced Materials". Furthermore, they wish to thank Mrs Rong Zhao and Dr Joseph Harris from the University of Erlangen-Nuremberg for Helpful comments.

Received 9 December 2015
Revised 26 April 2016
31 May 2016
Accepted 2 June 2016

Downloaded by FRIEDRICH ALEXANDER UNIVERSITAET ERLANGEN NUERNBERG At 09:18 10 June 2018 (PT)

hollow filaments, have been successfully cast by use of different extrusion nozzle shapes (Lewis, 2006). In particular, the hollow filament structure exhibits great potential for use in fabrication of lightweight materials with high mechanical performance (Abu-Absi *et al.*, 2005; Ahn *et al.*, 2005; Colombo *et al.*, 2003; Faiz *et al.*, 2013; Gardner *et al.*, 2001; Hoffman *et al.*, 1998; Konorov *et al.*, 2005; Lesage *et al.*, 2005; Yalin *et al.*, 2005; Yeo and Fane, 2005). However, robocasting of hollow filaments still remains a challenge because of their poor self-supporting properties during manufacturing (Schlordt *et al.*, 2013). Michielsen *et al.* (2013) successfully prepared stainless steel hollow fibers by means of a robotic fiber deposition technique with a special nozzle geometry. The rheological and drying behavior of the casting gels in addition to the casting gel feed speed and extrusion velocity were exactly controlled to avoid sample collapse during robocasting (Michielsen *et al.*, 2013). Moroni *et al.* (2006) fabricated fibers with a core-shell configuration by using two molten polymers with significantly different viscosities, which led to a viscous encapsulation effect during co-extrusion (Dooley, 2002); i.e. the polymer in the molten state with a lower viscosity tended to shift toward the walls of the duct when flowing through a narrow pipe, and therefore, fibers with a core-shell structure could be extruded (Dooley, 2002). Subsequently, after cooling, the inner core polymer was removed by selective dissolution and hollow polymeric fibers could be derived (Moroni *et al.*, 2006). In the present study, to manufacture hollow robocast filaments, carbon-Al_2O_3 core-shell filaments with different shell thickness were fabricated by means of a pressure-controlled piston co-extrusion process. After firing in air, the core material composed of the carbon gel was oxidized and evaporated, leaving ceramic fibers with a hollow cross-section. As the wall thickness was significantly affected by rheological properties of the core (carbon) and shell (alumina) gels and by material feed pressure during co-extrusion, the viscosity of both feedstock and the feed pressure for core and shell materials were investigated and optimized experimentally and numerically by computational fluid dynamics (CFD)-based simulation.

2. Experimental

2.1 Manufacturing of ceramic scaffolds with hollow and core-shell filaments

In this section, the experimental procedure to prepare 3D alumina lattice truss structures with hollow and core-shell filaments by means of a robocasting process combined with a co-extrusion technique will be presented. Figure 1 shows an overview of the process steps, which are explained in following sections in more detail.

2.1.1 Raw materials

To prepare gels for the robotically controlled co-extrusion, carbon (Luvomaxx N991, Lehmann & Voss & Co. KG, Hamburg, Germany) and Al_2O_3 (CT3000 SG, Almatis GmbH, Ludwigshafen, Germany) powders were used. The carbon powder showed a particle size between 0.4 and 0.8 μm ($\boldsymbol{d}_{10}$ = 0.43 μm, $\boldsymbol{d}_{50}$ = 0.51 μm and $\boldsymbol{d}_{90}$ = 0.60 μm) measured by laser granulometry (Mastersizer APA 2000, Malvern Instruments, London, Great Britain) and a specific surface area of 6.11 m^2/g derived from BET measurements (ASAP, 2000, Micromeritics, Norcross, GA USA), while the Al_2O_3 powder exhibited a slightly smaller particle size with $\boldsymbol{d}_{10}$ = 0.30 μm $\boldsymbol{d}_{50}$ = 0.35 μm and $\boldsymbol{d}_{90}$ = 0.42 μm and a higher specific surface area of 8.64 m^2/g.

Figure 1 Process flow diagram for fabrication of ceramic scaffolds with hollow and core-shell filaments

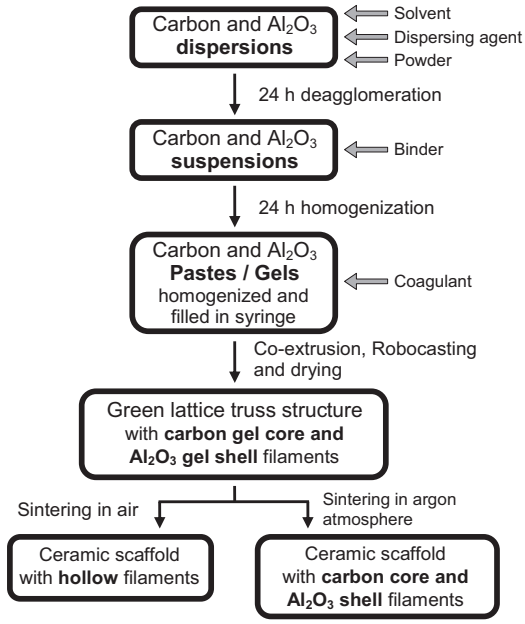

2.1.2 Colloidal gel preparation

For co-extrusion of filaments with core and shell configuration, two colloidal aqueous robocasting pastes composed of carbon and alumina particles were prepared, respectively. In both gels, the solid loading was kept at ~50 vol.% (Tables I and II). Based on former works (Schlordt *et al.*, 2012, 2013), Tables I and II show the exact composition used for the carbon and Al_2O_3 slurries and also the density of each component. During the preparation of carbon and Al_2O_3 gels, deionized water was used as a solvent. The dispersing agent and ceramic powder were first mixed with Al_2O_3 milling balls in a polyethylene (PE) bottle placed in a tumbling mixer (Turbula, Willy A. Bachofen AG, Muttenz, Switzerland) for 24 h at a mixing speed of 67 rpm. For the carbon dispersion, a solution mixture composed of 50 ma.% powdered Darvan 670 (electrosteric dispersant, sodium polynaphthalenesulfonate, R.T. Vanderbilt Co. Inc. Norwalk, CT, USA) and 50 ma.% deionized water was used as dispersant (Table I), while to disperse Al_2O_3 particles, a Darvan C-N dispersant solution (electrosteric dispersant, ammonium salt of polymethacrylic acid, R.T. Vanderbilt Co. Inc. Norwalk, CT, USA) was added into the aqueous alumina dispersion. Subsequently, binder was added into both dispersions. For the case of carbon dispersion, powdered PEG (polyethylene glycol, molar weight of ~10,000, Merck Schuchardt OHG, Hohenbrunn Germany) served as a binder, while in the Al_2O_3 dispersion, a binder solution composed of 10 ma.% powdered PEO (polyethylene oxide, molar weight of ~400,000, Sigma-Aldrich Co. St. Louis, MO, USA) and 90 ma.% deionized water was used. This binder-assisted

Downloaded by FRIEDRICH ALEXANDER UNIVERSITAET ERLANGEN NUERNBERG At 09:18 10 June 2018 (PT)

Table I Composition of the carbon gel (core feedstock) for robotically controlled co-extrusion

Steps of slurry preparation	Raw materials	Function of added materials	Volume fraction (vol.%)	Mass fraction (ma.%)	Density[a] (g/cm^3)
Carbon gel (paste)					
Suspension					
Dispersion	Carbon powder	Ceramic powder	48.6	63.1	1.8
	Dispersing agent solution (mixture of 50 ma.% powdered Darvan 670 and 50 ma.% water)	Dispersant	0.7	0.5	1.1*
	Deionized water	Solvent	37.4	26.1	1.0
	Powdered PEG	Binder	3.9	3.2	1.2
	Ammonium acetate solution (composed of 66.6 ma.% powdered CH_3COONH_4 and 33.4 ma.% water)	Coagulant	5.9	4.6	1.1*
	Deionized water	Solvent	3.5	2.5	1.0

Notes: [a]Density values calculated or give by the data from producers; *powdered Darvan 670 and ammonium acetate show density values of 1.3 g/cm^3 and 1.2 g/cm^3, respectively

Table II Composition of the Al_2O_3 gel (shell feedstock) for robotically controlled co-extrusion

Steps of slurry preparation	Raw materials	Function of added materials	Volume fraction (vol.%)	Mass fraction (ma.%)	Density[a] (g/cm^3)
Alumina gel (paste)					
Suspension					
Dispersion	Al_2O_3 powder	Ceramic powder	50.3	79.7	4.0
	Darvan C-N solution (mixture of 25 ma.% powdered Darvan C-N and 75 ma.% water)	Dispersant	5.4	2.4	1.1
	Deionized water	Solvent	34.0	13.6	1.0
	PEO binder solution (composed of 10 ma.% powdered PEO and 90 ma.% water)	Binder	4.7	1.9	1.0*
	Ammonium acetate solution (composed of 66.6 ma.% powdered CH_3COONH_4 and 33.4 ma.% water)	Coagulant	3.9	1.7	1.1
	Deionized water	Solvent	1.7	0.7	1.0

Notes: [a]Density values calculated or give by the data from producers; *powdered PEO binder shows a density of 1.2 g/cm^3

suspension was homogenized for an additional 24 h. Finally, a solution mixture composed of 66.6 ma.% powdered ammonium acetate (CH_3COONH_4, Merck KGaA, Darmstadt, Germany) and 33.4 ma.% deionized water was added into both slurries as coagulant; at the same time, additional solvent (deionized water) was also added into the final carbon and Al_2O_3 pastes to adjust the solid loading and the rheological behavior. Before co-extrusion, the two robocasting gels were sieved to remove milling balls and then drawn into syringes. To ensure high homogeneity and bubble-free pastes, homogenization and degassing of both the syringe-filled gels were then performed by means of a centrifugal planetary mixer (ARE-250, Thinky Co., Tokyo, Japan).

2.1.3 Co-extrusion integrated robocasting

The manufacturing of green scaffolds with carbon-alumina core-shell filaments was performed by a six-axis robocasting system (RobFab, Battenberg ROBOTIC GmbH & Co. KG, Marburg, Germany) equipped with a piston co-extrusion unit, which consisted of a stainless steel casing, feed pipes for core (carbon gel) and shell (alumina gel) materials, a long feed capillary for the core paste and an extrusion nozzle with an inner diameter of 1.5 mm [Figure 2(a) and (b)]. During co-extrusion, the feed speed of carbon and alumina gels was controlled by alteration of gas pressure; i.e. the wall thickness and the core diameter of the final co-extrusion products as well as the extrusion velocity of core-shell filaments could quantitatively be controlled by setting the core and shell feed pressure. In this study, three different setups of gas pressure were applied on the core and shell side: 1.4/1.8, 1.4/2.3 and 1.6/2.1; the number in front of the slash symbol represents the core pressure in 10^5 Pascal, while the number behind the slash denotes the shell pressure in 10^5 Pascal (Table IV). Furthermore, the wall thickness of the filaments cast under different pressure conditions was determined by image analysis (Section 2.2.2). The extrusion velocity U of core-shell

Downloaded by FRIEDRICH ALEXANDER UNIVERSITAET ERLANGEN NUERNBERG At 09:18 10 June 2018 (PT)

Figure 2 Geometry of the pressure-controlled piston co-extrusion unit, which is integrated in the robocasting system

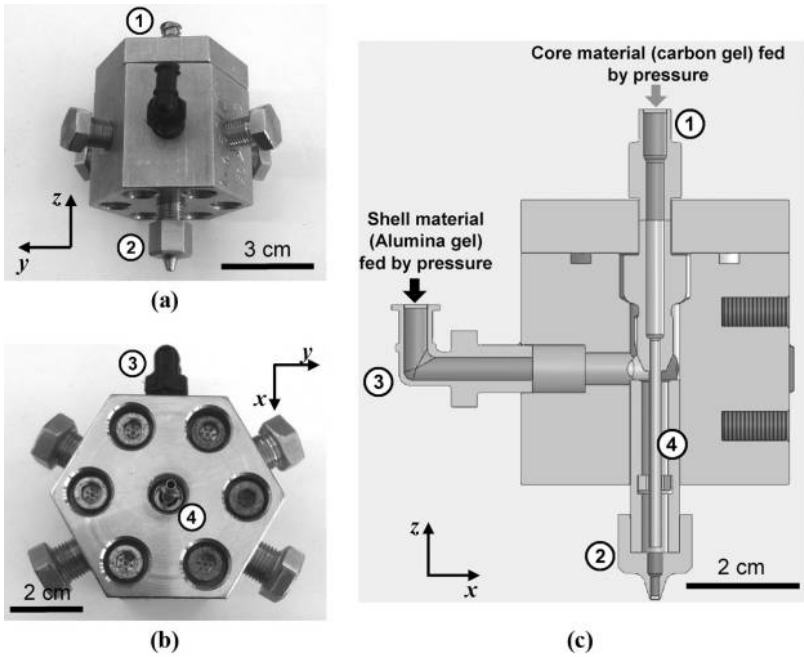

Notes: (a) and (b) side and bottom view of the real piston co-extrusion unit. (c): cutaway view of the 3D modeling. The numbers represent different components: ① feed duct for core material, ② extrusion nozzle, ③ feed duct for shell material and ④ feed capillary for core material

fibers after the nozzle exit was also experimentally measured by stopper and caliper; i.e. the time, which was needed to extrude a filament with a certain length (e.g. 50 mm), was recorded by stopper. To have a better understanding and control of the pressure-controlled co-extrusion, the whole process was also numerically simulated by an open-source CFD software "OpenFoam" (www.openfoam.org); additionally, the numerically calculated wall thickness was compared to that derived experimentally (Sections 2.2.2 and 2.2.3). For this purpose, the real structure of the piston co-extrusion unit was computationally reconstructed by commercial computer-aided design software "Solid Edge" (Siemens PLM Software, Köln, Germany) [Figure 2(c)].

Robocasting took place under controlled external conditions at a temperature of 20 ± 2°C. The moving speed of the robot arm was set so that it was equal to the filament extrusion rate (between 3 and 7 mm/s). The structures was deposited on a smooth alumina substrate (Kerafol GmbH, Eschenbach, Germany), which was immersed in an oil bath (Oil S.5585, Deutsche Shell Holding, Hamburg, Germany) (Schlordt *et al.*, 2012). After the robotic co-extrusion, 3D macro-cellular lattice truss structures with continuous carbon core and alumina shell filaments were fabricated. Drying of the robocast green structures occurred in air at a constant temperature of ~20°C for 24 h.

2.1.4 Thermal treatments

To obtain ceramic scaffolds with hollow filaments, the dried green structures were fired in air (with furnace HT16/17, Nabertherm GmbH, Lilienthal, Germany). According to thermal gravimetric analysis (STA 429, Netzsch, Selb, Deutschland), carbon and all organic substances should be totally burnt out above 1,000°C in air (Vilčáková *et al.*, 2012). Thus, debinding and carbon burnout took place in air with a heating rate of 2 K/min up to 1,000°C, followed by sintering at 1,600°C with a holding time of 2 h and a heating rate of 5 K/min. At the same time, the green scaffolds were also pyrolyzed and sintered in an argon atmosphere with the same thermal treatment profile as sintered in air (with furnace HTRH 100/300-18, GERO Hochtemperaturöfen GmbH & Co. KG, Neuhausen, Germany). After firing in argon, the carbon core remained and scaffolds with a carbon core and alumina shell filaments were derived.

2.2 Characterization

2.2.1 Rheological properties

Before robocasting, the rheological behavior of carbon and alumina gels was measured by MCR 302 viscometer (Anton Paar Germany GmbH, Ostfildern, Germany) at 20°C in a confined space. To determine the viscosity η as a function of shear rate $\dot{\gamma}$, which varied in a range between 1 s^{-1} and 200 s^{-1}, a cone-plate measuring system with a sandblasted cone (diameter: 25 mm, cone angle: 1°) and plate was used, where the gap height was adjusted to 50 μm. Furthermore, to have an analytical description of the rheological properties of both non-Newtonian pastes, the Cross viscosity model was used (Cross, 1965; Wonisch *et al.*, 2011):

$$\eta(\dot{\gamma}) = \eta_{\infty} + \frac{\eta_0 - \eta_{\infty}}{1 + (m \cdot \dot{\gamma})^n} \quad (1)$$

Downloaded by FRIEDRICH ALEXANDER UNIVERSITAET ERLANGEN NUERNBERG At 09:18 10 June 2018 (PT)

where $\eta(\dot{\gamma})$ denotes the shear rate-dependent viscosity; $\dot{\gamma}$ represents the shear rate; η_∞ and η_0 are the viscosity at zero shear rate and at a shear rate which tends to infinity, respectively; m (which is always greater than zero) and n ($n > 0$: shear-thinning, $n < 0$: shear-thickening) are material constants of the gels. The parameters for the Cross model were experimentally determined by viscometery and used in the numerical simulation (Section 2.2.3).

2.2.2 Microstructural analysis

To determine the pressure-dependent diameter of the core (t) and the whole filament (D) and because the mechanical strength of the green structures was not sufficient for the preparation of polished cross-sections for SEM analysis, cross-sections of filaments sintered in air were analyzed by scanning electron microscopy (SEM, Quanta 200, FEI Ltd, Hillsboro, OR, USA). Before SEM analysis, the fired samples were polished with a 1 μm diamond finish and sputtered with gold. For image analysis, all SEM micrographs were converted into binary pictures [Figure 3(a) and (b)] using the software ImageJ (National Institute of Health, Bethesda, MD, USA). During the binary conversion, the default setting in the program ImageJ was used for the gray scale threshold. The core and filament diameters, t and D, were determined by the so-called "best-fit ellipse method" (Fu and Roosen, 2015); i.e. every annular filament cross-section is approximated by two ring-like best-fit ellipses [inner ellipse represents the core, outer ellipse the shell; see Figure 3(c)]. Average length of the minor and major axis of the inner fitted ellipse was considered to be the core diameter (t). The filament diameter (D) could be measured accordingly by analyzing the outer ellipse. Average t and D values were calculated from measurements of at least 30 different annular filament cross-sections. Furthermore, the area of the inner and outer ellipses was measured by image analysis to calculate the core area fraction (S_c) in the whole filament cross-section. Moreover, the porosity in hollow alumina struts was determined by calculating the area fraction of the pores.

Figure 3 Procedure of image analysis to measure the core and shell diameter (t and D) as well as the core area fraction (S_c) in filament cross-sections after sintering a): original SEM-picture, b): SEM-picture after binary conversion and c): after best-fit ellipse method

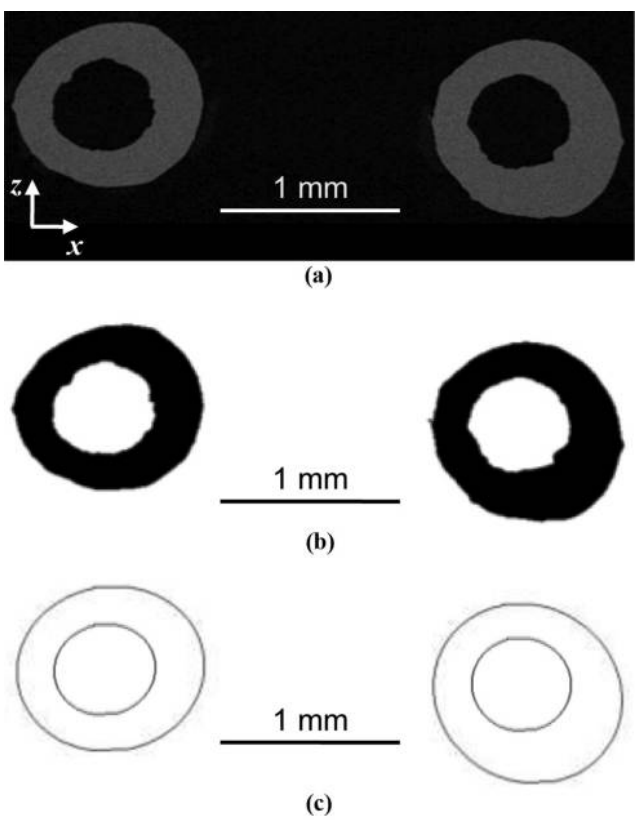

2.2.3 Numerical investigation

As mentioned in Section 2.1.3, the co-extrusion process was also numerically simulated by "OpenFoam" software to study the pressure-dependent wall thickness. The flow simulation is based on the solving of the Navier–Stoke's equation (Constantin and Foias, 1988). In this study, the solver "InterFoam" integrated in "OpenFoam" was used, which is based on the volume of fluid (VOF) method to determine the relative volume fraction of the two phases in each computational cell (www.openfoam.org). The use of the VOF method means that an interface between the fluids is not explicitly computed, but rather emerges as a property of the phase fraction field; i.e. the interface is not sharply defined but occupies a volume around the region where a sharp interface should exist (www.openfoam.org). The "InterFoam" solver was suitable for the flow behavior investigation of two incompressible, isothermal and immiscible fluids (Deshpande *et al.*, 2012; Shonibare and Wardle, 2015). To describe the flow behavior as well as rheological properties, both gels were assumed to follow Cross viscosity model.

3. Results and discussion

3.1 Rheological properties of robocasting gels

Figure 4 shows the viscosity as a function of shear rate of carbon and alumina robocasting gels for co-extrusion. Owing to the different particle geometries and surface chemistries of

Figure 4 Experimentally measured rheological properties of the carbon and alumina gels as a function of shear rate; and fitting curves according to the Cross model using the method of least squares

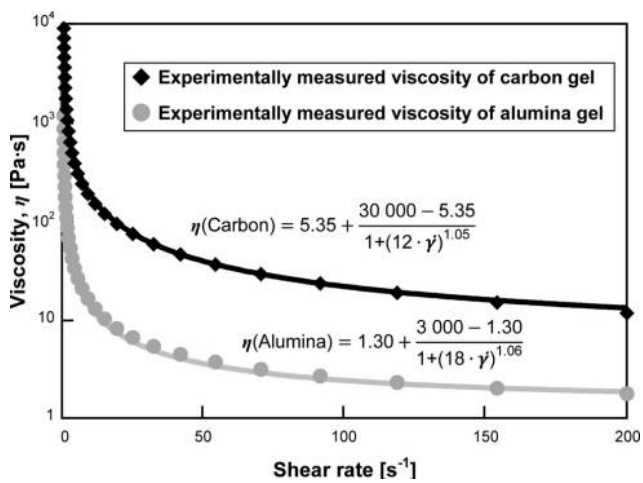

Downloaded by FRIEDRICH ALEXANDER UNIVERSITAET ERLANGEN NUERNBERG At 09:18 10 June 2018 (PT)

carbon and alumina powders, the carbon gel exhibited a significantly higher viscosity than that of the alumina gel (Figure 4). This phenomenon benefited the co-extrusion process with a carbon gel core and alumina gel shell because of the so-called viscous encapsulation effect as mentioned in Section 1 and reported by Moroni *et al.* (2006). Owing to the higher shear stress at duct walls, the alumina slurry with lower viscosity shifted automatically toward the walls and resulted in a core-shell structure (Moroni *et al.*, 2006). As mentioned in Section 2.2.1, the rheological properties of both non-Newtonian fluids were also analytically described by Cross model, Equation (1). By fitting the viscosity/shear rate curves in Figure 4, parameters in Equation (1) were calculated and shown in Table III. The parameters of the Cross model for both pastes shown in Figure 4 were used as input for the CFD simulation (Section 3.2).

3.2 Wall thickness

In this study, to investigate the wall thickness of the core-shell filaments in dependence on co-extrusion parameters, different setups of gas pressure were applied on the core and shell side. As explained in Section 2.1.3, three different setups were used for experimental and numerical study (see also Table IV). In Figure 5(a), (b) and (c), SEM images of cross-sections of filaments extruded under different core and shell pressures and sintered in air are shown. In Setups 1 and 3 with core and shell pressure of $1.4/1.8 \times 10^5$ Pa and $1.6/2.1 \times 10^5$ Pa, respectively, similar wall thickness was observed [Figure 5(a) and (c)]; however, in Setup 2, the wall thickness seemed to be significantly higher [Figure 5(b)]. This SEM observation in Figure 5 was confirmed with the results derived by image analysis shown in Table IV. Setups 1 and 3 exhibited similar t, D and S_c-values; in contrast, t and S_c in Setup 2 showed significantly lower values because of higher difference in core and shell pressure. Furthermore, during experimental and numerical study it was found, if the core-shell pressure difference would be set too high, either only a pure black carbon or white alumina fiber would be extruded from the nozzle exit. At the same time, it was noticeable that in Setups 1 and 3 [Figure 5(a) and (c)] almost straight vertical struts were formed, whereas when Setup 2 [Figure 5(b)] was used, clear strut deflection was evident. This strut deflection phenomenon has also been previously reported during robocasting of scaffolds (Schlordt *et al.*, 2012). Schlordt *et al.* (2012) calculated the deflection of pure alumina fibers analytically and found that the deflection was strongly dependent on the paste viscosity; with decreasing viscosity, the deflection displacement increased. In the case of the core-shell filaments co-extruded in this study, the strut deflection problem is much more complicated. The degree of strut deflection was found to be governed by the quantity of the most viscous component. As the alumina shell paste had a significantly lower viscosity than the carbon core gel, strut deflection was related to the quantity of carbon gel (core volume). With increasing carbon core gel content, less strut deflection was observed, which resulted in the interesting property that decreasing wall thickness gave structures with less strut deflection (Figure 5).

The relationship between the extrusion velocity U and the core and shell pressures was also experimentally analyzed (Table IV). This was achieved by freely co-extruding the pastes for 10 cm and simultaneously recording the time; however, zigzag flow in radial directions (x and y direction in Figure 2) and flow toward one radial direction were often observed, which made the experimental measurement of casting speed much harder. Therefore, the extrusion velocity values observed in Table IV are approximate. Setups 2 and 3 showed similar extrusion velocities; however, a lower casting speed was observed in Setup 1 because of lower total pressure applied on the core and shell side (Table IV).

Furthermore, the carbon gel content in the extruded filament cross-section was also numerically studied using the same experimental setups and viscosity data shown in Section 3.1. Table IV shows the numerically calculated volume fraction of carbon gel S_c' at the nozzle exit. Compared to the experimentally measured S_c-values (hollow core area fraction

Table III Cross model parameters [Equation(1)] Used for numerical modelling

Parameters	Carbon gel	Alumina gel
η_∞ (Pa·s)	5.35	1.30
η_0(Pa·s)	30,000	3,000
m (s)	12	18
n	1.05	1.06

Table IV Experimentally and numerically derived core and shell diameter in dependence on core and shell pressure during co-extrusion

Setups	Core pressure (10^5 Pa)	Shell pressure (10^5 Pa)	Experimentally measured core diameter, t (mm)	Experimentally measured filament diameter, D (mm)	Experimentally measured core area fraction in filament cross-sections after firing in air, S_C	Experimentally measured extrusion velocity, U (filament exiting speed) (mm/s)	Numerically derived and processing time-dependent carbon gel content (S_c') in fluid at the nozzle exit	Numerically derived and processing time-dependent extrusion velocity in the z-direction at the nozzle exit, U_z (mm/s)
Setup 1								
1.4/1.8	1.4	1.8	0.55 ± 0.07	1.06 ± 0.08	27.4% ± 7.1%	~3.6	16.7% ± 8.2%	23.4 ± 0.2
Setup 2								
1.4/2.3	1.4	2.3	0.38 ± 0.06	1.18 ± 0.12	10.9% ± 3.7%	~6.3	4.7% ± 3.5%	43.3 ± 0.1
Setup 3								
1.6/2.1	1.6	2.1	0.56 ± 0.04	1.04 ± 0.08	29.1% ± 4.5%	~5.7	20.2% ± 8.3%	36.3 ± 0.2

Downloaded by FRIEDRICH ALEXANDER UNIVERSITAET ERLANGEN NUERNBERG At 09:18 10 June 2018 (PT)

Figure 5 Wall thickness of filaments extruded under different core and shell feed pressures

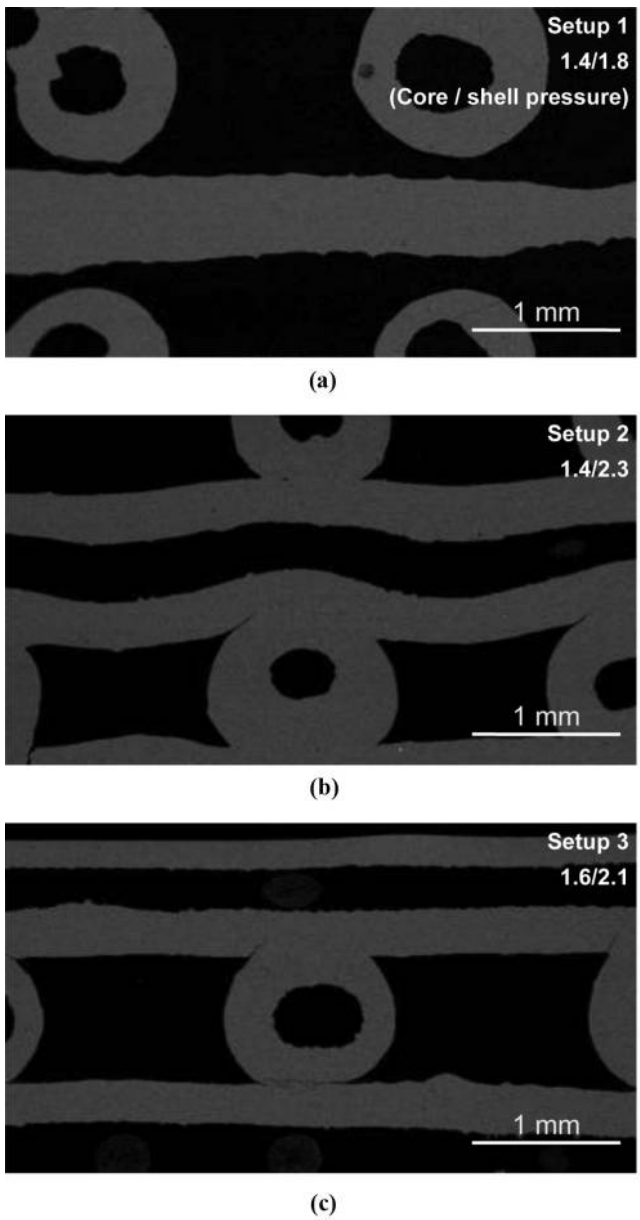

Notes: (a), (b) and (c) experimentally derived SEM cross-sections of filaments sintered in air

in the filament cross-section after firing), the simulated S_c'-values (carbon core fraction in fluid at the nozzle exit before drying and firing) were always smaller (Table IV). As mentioned in Section 2.2.2, during experimental investigation, the green structures were not strong enough for the preparation of polished cross-sections for SEM analysis; therefore, S_c'-values had to be calculated by simulation. Fired filaments were strong enough for SEM examination; therefore, S_c-values were calculated from experimental data. In numerical simulation, to determine the core area variation after drying and thermal treatments, new analytical or numerical modeling would be required; this would be beyond the scope of this work. The difference between S_c and S_c' can be explained by the model in Figure 6. After binder and carbon core burnout above ~1,000°C in air, the shrinkage of the alumina shell occurs (Figure 6). Assuming that during sintering shrinkage of the alumina layer occurs toward the center of the layer (termed neutral phase in Figure 6), the core area increases in cross-sectional area, while the overall diameter of the filament decreases. This results in a significant increase of the core area fraction of the whole cross-section after firing (Figure 6). Therefore the S_c-values after sintering were greater than the S_c'-values in the green state. In addition, during sintering, a slightly anisotropic shrinkage behavior was found; e.g. the sintering shrinkage in the z-direction was slightly higher than that in the x-direction (see the coordination system in Figures 2 and 6). Nevertheless, the experimentally and numerically derived S_c- and S_c'-values showed good qualitative agreement; with increasing difference in core and shell pressure, a decrease was observed in both S_c and S_c'.

Figure 7 shows representative numerical results, e.g. carbon gel concentration [Figure 7(a)], pressure [Figure 7(b)] and velocity distribution [Figure 7(c)] in the whole co-extrusion unit for the case of Setup 3 with a core and shell pressure of 1.6×10^5 Pa and 2.1×10^5 Pa during robocasting. A limitation of the CFD-simulation solver is that in the nozzle area an undesired mixing of core and shell pastes was observed which is not seen experimentally [Figure 7(a)]; thus, the numerically calculated filament extrusion velocity at the nozzle exit and the viscosity of the mixture in the nozzle area could differ from those of the real core-shell filaments extruded experimentally in which a clear interface between core and shell was observed. In the simulation, in the z-direction along the nozzle, almost the same carbon gel content in fluids was detected and a homogenization occurred, i.e. the mixing of the core and shell gels did not significantly

Figure 6 Filament cross-section before and after sintering in air. Shrinkage of the alumina shell toward the central neutral phase during sintering decreases the shell fraction and increases the core fraction; therefore, the S_c-value (hollow core area fraction in the filament cross-section after sintering) is greater than the S_c'-value (carbon core area fraction in green state)

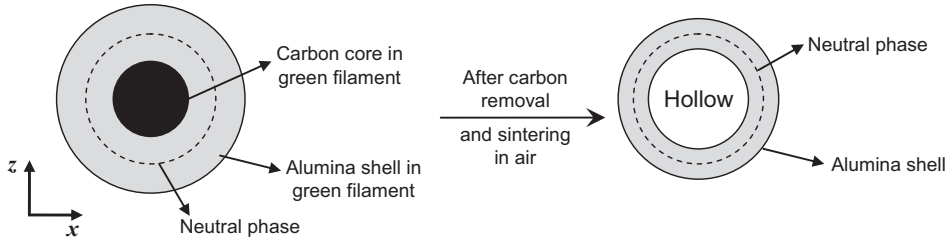

Downloaded by FRIEDRICH ALEXANDER UNIVERSITAET ERLANGEN NUERNBERG At 09:18 10 June 2018 (PT)

Figure 7 Representative simulated carbon gel concentration (a), pressure (b) and paste velocity (c) distribution in the whole co-extrusion unit for the case of Setup 3 with a core and shell pressure of 1.6 × 10^5 Pa and 2.1 × 10^5 Pa

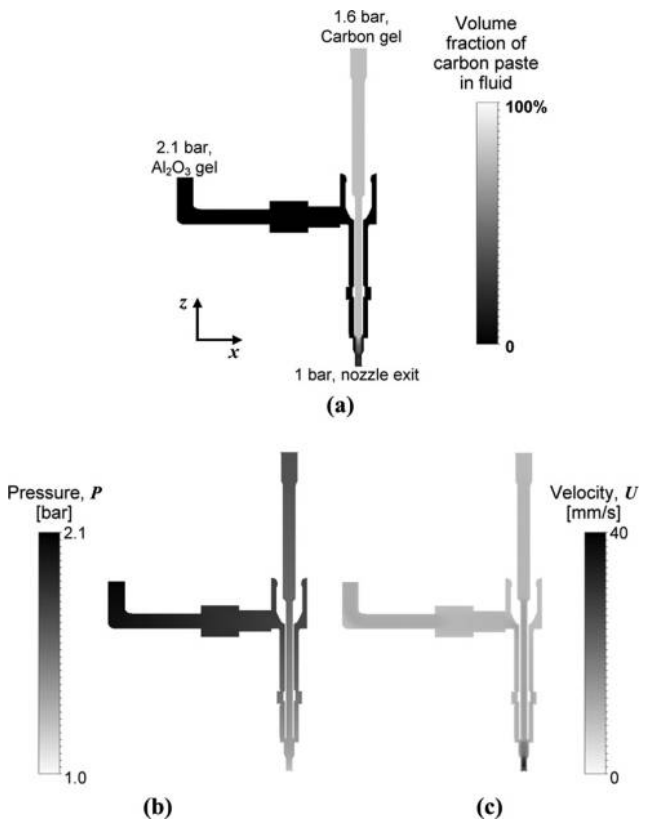

affect the composition in core-shell filaments. As discussed above and shown in Table IV, the experimentally and numerically derived S_c- and S_c'-values showed good qualitative accordance with each other. Theoretically, a more exact co-extrusion simulation could be achieved to calculate the extruded filament diameter by using the no-cross-flow condition at the interface of both fluids. But in this case, a new algorithm and computational coding would be required for multiphase flow simulation, which will be further investigated in future works. According to the numerical simulation, the pressure and paste velocity distribution in the co-extrusion unit stayed almost constant [Figure 7(b) and (c)]. In addition, the numerically calculated extrusion speed in the z-direction, U_z (see the coordination system in Figure 2), is also shown in Table IV. Compared to the experimentally measured filament velocity, U, the numerical simulation showed higher extrusion velocity. This difference could be explained by following aspects. First, to reduce the computational effort during simulation, the geometry of the co-extrusion unit was simplified during modeling, e.g. small gaps between different parts of the co-extrusion unit were not taken into account. Furthermore, during the experiment, both pastes were drawn into syringes, which were placed on the co-extrusion unit; and the feed pressure was directly applied to both syringes, which were not modeled in the numerical study. Second, as discussed above, the interaction of both gels on the interface was hard to be defined. Third, as mentioned previously, the reliability level of the experimentally detected filament extrusion velocity was not high because of the zigzag flow in lateral directions. Based on these factors, the experimentally and numerically derived filament velocity in the z-direction (see the coordination system in Figure 2) could differ from each other. However, the experimentally and numerically derived U and U_z showed qualitative agreement, i.e. the extrusion speed increased with feed pressure. Moreover, in Table IV, it is noticeable that the experimentally measured and numerically calculated S_c and S_c' exhibited high deviation. Figure 8 shows the exact paste velocity at the nozzle exit in all three spatial directions as a function of extrusion time for the case of Setup 3 with a core and shell pressure of 1.6 × 10^5 Pa and 2.1 × 10^5 Pa. After a given extrusion time, the three U-curves leveled off, and during the entire extrusion process U_x and U_y in lateral directions stayed almost at zero (Figure 8). However, high fluctuation was observed in all three U-curves (Figure 8). This phenomenon could be explained by the turbulence effect in the nozzle area [Figure 7(c)], in which high paste speed was observed. To reduce this fluctuation in extrusion velocity and that of the S_c-values, the Reynolds number, R_e in the co-extrusion unit should be minimized (e.g. by reduction of extrusion velocity and nozzle diameter or by the enhancement of paste viscosity).

3.3 Robocast lattice truss structure

After robocasting and sintering in air, all samples with different setups exhibited almost the same alumina strut microstructure with a porosity of ~1 per cent (Figure 9).

In addition, smaller structures with a filament diameter of ~0.4 mm extruded by a nozzle with an inner diameter of 0.5 mm were also fabricated (Figure 10). Furthermore, as mentioned in Section 2.1.4, green robocast structures were also fired in argon to prevent oxidation of the carbon core; hence, filaments with a carbon core and Al_2O_3 shell configuration were derived after sintering. Figure 11 shows cross-sections of these smaller scaffolds fired in air and in argon.

Figure 8 Numerically calculated extrusion velocity U in all three spatial directions (see the coordination system in Figure 2) at the nozzle exit as a function of processing time for the case of Setup 3 with a core and shell pressure of 1.6 × 10^5 Pa and 2.1 × 10^5 Pa

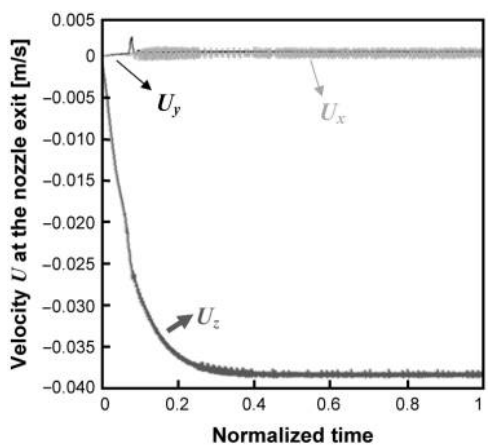

Downloaded by FRIEDRICH ALEXANDER UNIVERSITAET ERLANGEN NUERNBERG At 09:18 10 June 2018 (PT)

Figure 9 Microstructure of alumina struts fired in air at 1,600°C with a porosity of ~1.4 per cent

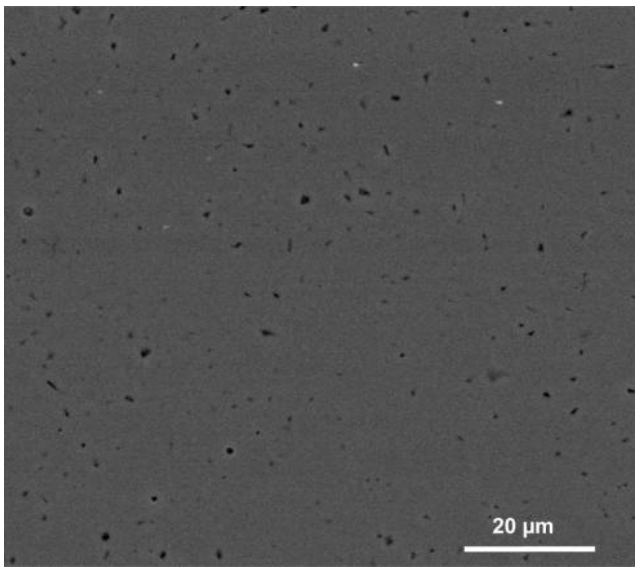

Figure 10 Macrostructure of robocast ceramic scaffolds with a nozzle diameter of 0.5 mm

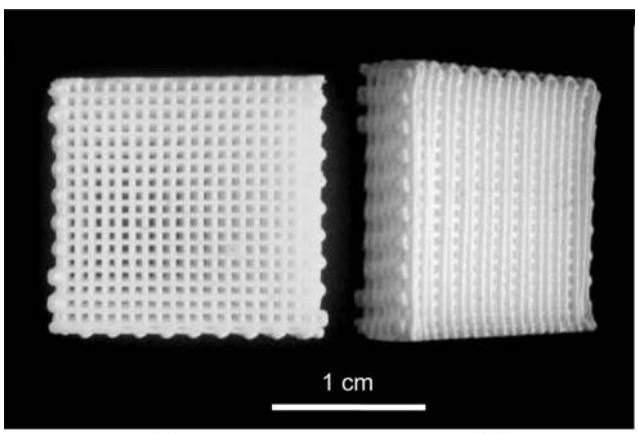

Notes: (a) Top view; (b) Isometric view

4. Conclusion

Green lattice truss structures with carbon core and alumina shell filaments were successfully manufactured by robotically controlled co-extrusion. As feedstocks carbon and alumina gels with significantly different rheological properties were prepared. During co-extrusion, the core paste exhibited a much higher viscosity than the shell paste, which benefited the co-extrusion process. Simultaneously, the core and shell diameters were controlled by core and shell feed pressures and studied by numerical simulation. The experimentally and numerically derived filament wall thickness showed qualitative agreement with each other; with decreasing core pressure during co-extrusion, the wall thickness increased. Furthermore, structures with different filament diameters were fabricated by using different nozzle diameters (1.5 and 0.5 mm). After firing in air, in which the carbon core was burnt out, hollow filament scaffolds were obtained; however, the carbon core remained in the Al_2O_3 shell after firing in an argon atmosphere.

Figure 11 Cross-sections of 3D lattice truss structures with a filament diameter of ~0.4 mm

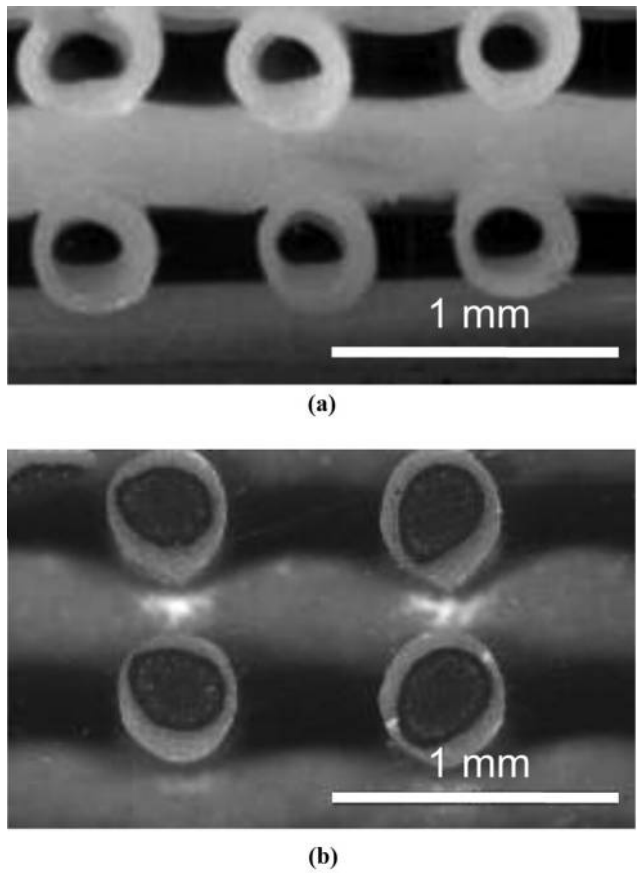

Notes: (a) Structure sintered in air with hollow filaments; (b) Structure sintered in argon with carbon-alumina core-shell filaments

References

Abu-Absi, S.F., Seth, G., Narayanan, R.A., Groehler, K., Lai, P., Anderson, M.L., Sielaff, T. and Hu, W.S. (2005), "Characterization of a hollow fiber bioartificial liver device", *Artificial Organs*, Vol. 29 No. 5, pp. 419-422.

Ahn, B.Y., Walker, S.B., Slimmer, S.C., Russo, A., Gupta, A., Kranz, S., Duoss, E.B., Malkowski, T.F. and Lewis, J.A. (2011), "Planar and three-dimensional printing of conductive inks", *Journal of Visualized Experiments: JoVE*, Vol. 58.

Ahn, Y.H., Bensadoun, J.C., Aebischer, P., Zurn, A.D., Seiger, Å., Björklund, A., Lindvall, O., Wahlberg, L., Brundin, P. and Schierle, G.S.K. (2005), "Increased fiber outgrowth from xeno-transplanted human embryonic dopaminergic neurons with co-implants of polymer-encapsulated genetically modified cells releasing glial cell line-derived neurotrophic factor", *Brain Research Bulletin*, Vol. 66 No. 2, pp. 135-142.

Downloaded by FRIEDRICH ALEXANDER UNIVERSITAET ERLANGEN NUERNBERG At 09:18 10 June 2018 (PT)

Cesarano, J., Segalman, R. and Calvert, P. (1998), "Robocasting provides moldless fabrication form slurry deposition", *Ceramic Industry*, Vol. 148, p. 94.

Colombo, P., Perini, K., Bernardo, E., Capelletti, T. and Maccagnan, G. (2003), "Ceramic microtubes from preceramic polymers", *Journal of the American Ceramic Society*, Vol. 86 No. 6, pp. 1025-1027.

Constantin, P. and Foias, C. (1988), *Navier-Stokes Equations*, University of Chicago Press, Chicago.

Cross, M.M. (1965), "Rheology of Non-Newtonian fluids: a new flow equation for pseudoplastic systems", *Journal of Colloid Science*, Vol. 20 No. 5, pp. 417-437.

de Hazan, Y., Thänert, M., Trunec, M. and Misak, J. (2012), "Robotic deposition of 3d nanocomposite and ceramic fiber architectures via UV curable colloidal inks", *Journal of the European Ceramic Society*, Vol. 32 No. 6, pp. 1187-1198.

Deshpande, S.S., Anumolu, L. and Trujillo, M.F. (2012), "Evaluating the performance of the two-phase flow solver interFoam", *Computational Science & Discovery*, Vol. 5 No. 1, p. 014016.

Doiphode, N., Huang, T., Leu, M., Rahaman, M. and Day, D. (2011), "Freeze extrusion fabrication of 13–93 bioactive glass scaffolds for bone repair", *Journal of Materials Science: Materials in Medicine*, Vol. 22 No. 3, pp. 515-523.

Dooley, J. (2002), *Viscoelastic Flow Effects in Multilayer Polymer Coextrusion*, Technische Universiteit Eindhoven, Eindhoven.

Faiz, R., Fallanza, M., Ortiz, I. and Li, K. (2013), "Separation of olefin/paraffin gas mixtures using ceramic hollow fiber membrane contactors", *Industrial & Engineering Chemistry Research*, Vol. 52 No. 23, pp. 7918-7929.

Fu, Z. and Roosen, A. (2015), "Shrinkage of tape cast products during binder burnout", *Journal of the American Ceramic Society*, Vol. 98 No. 1, pp. 20-29.

Fu, Z., Schlier, L., Travitzky, N. and Greil, P. (2013), "Three-dimensional printing of SiSiC lattice truss structures", *Materials Science and Engineering: A*, Vol. 560, pp. 851-856.

Gardner, T., Ko, S., Yang, L., Cadwell, J., Chung, L. and Kao, C. (2001), "Serum-free recombinant production of adenovirus using a hollow fiber capillary system", *Biotechniques*, Vol. 30 No. 2, pp. 422-427.

Gratson, G.M., Xu, M. and Lewis, J.A. (2004), "Microperiodic structures: direct writing of three-dimensional webs", *Nature*, Vol. 428 No. 6981, p. 386.

He, G., Hirschfeld, D.A., Cesarano, J. and Stuecker, J.N. (2008), "Robocasting and cofiiung of functionally graded Si3N4-W materials", *25th Annual Conference on Composites, Advanced Ceramics, Materials, and Structures: B: Ceramic Engineering and Science Proceedings*, *John Wiley & Sons, New York, NY*, pp. 119-125.

Hoffman, W.P., Phan, H.T. and Wapner, P.G. (1998), "The far-reaching nature of microtube technology", *Material Research Innovations*, Vol. 2 No. 2, pp. 87-96.

Konorov, S., Serebryannikov, E., Fedotov, A., Miles, R. and Zheltikov, A. (2005), "Phase-matched waveguide four-wave mixing scaled to higher peak powers with large-core-area hollow photonic-crystal fibers", *Physical Review E*, Vol. 71 No. 5, p. 057603.

Lesage, N., Sprandio, M. and Cabassud, C. (2005), "Performances of a hybrid adsorption/submerged membrane biological process for toxic waste removal", *Water Science & Technology*, Vol. 51 Nos 6/7, pp. 173-180.

Lewis, J.A. (2006), "Direct ink writing of 3D functional materials", *Advanced Functional Materials*, Vol. 16 No. 17, pp. 2193-2204.

Lewis, J.A., Smay, J.E., Stuecker, J. and Cesarano, J. III (2006), "Direct ink writing of three-dimensional ceramic structures", *Journal of the American Ceramic Society*, Vol. 89 No. 12, pp. 3599-3609.

Li, J., De Wijn, J., Van Blitterswijk, C. and De Groot, K. (2010), "The effect of scaffold architecture on properties of direct 3D fiber deposition of porous Ti6Al4V for orthopedic implants", *Journal of Biomedical Materials Research Part A*, Vol. 92 No. 1, pp. 33-42.

Lorang, D.J., Tanaka, D., Spadaccini, C.M., Rose, K.A., Cherepy, N.J. and Lewis, J.A. (2011), "Photocurable liquid core–fugitive shell printing of optical waveguides", *Advanced Materials*, Vol. 23 No. 43, pp. 5055-5058.

Mason, M.S., Huang, T., Landers, R.G., Leu, M.C. and Hilmas, G.E. (2009), "Aqueous-based extrusion of high solids loading ceramic pastes: process modeling and control", *Journal of Materials Processing Technology*, Vol. 209 No. 6, pp. 2946-2957.

Michielsen, B., Chen, H., Jacobs, M., Middelkoop, V., Mullens, S., Thijs, I., Buekenhoudt, A. and Snijkers, F. (2013), "Preparation of porous stainless steel hollow fibers by robotic fiber deposition", *Journal of Membrane Science*, Vol. 437 No. 17, pp. 17-24.

Miranda, P., Saiz, E., Gryn, K. and Tomsia, A.P. (2006), "Sintering and robocasting of β-tricalcium phosphate scaffolds for orthopaedic applications", *Acta Biomaterialia*, Vol. 2 No. 4, pp. 457-466.

Morissette, S.L., Lewis, J.A., Cesarano, J. III, Dimos, D.B. and Baer, T.A. (2000), "Solid freeform fabrication of aqueous alumina-poly (vinyl alcohol) gelcasting suspensions", *Journal of the American Ceramic Society*, Vol. 83 No. 10, pp. 2409-2416.

Moroni, L., Schotel, R., Sohier, J., de Wijn, J.R. and van Blitterswijk, C.A. (2006), "Polymer hollow fiber three-dimensional matrices with controllable cavity and shell thickness", *Biomaterials*, Vol. 27 No. 35, pp. 5918-5926.

Nadkarni, S.S. and Smay, J.E. (2006), "Concentrated barium titanate colloidal gels prepared by bridging flocculation for use in solid freeform fabrication", *Journal of the American Ceramic Society*, Vol. 89 No. 1, pp. 96-103.

Roberson, D., Shemelya, C.M., MacDonald, E. and Wicker, R. (2015), "Expanding the applicability of FDM-type technologies through materials development", *Rapid Prototyping Journal*, Vol. 21 No. 2, pp. 137-143.

Saiz, E., Gremillard, L., Menendez, G., Miranda, P., Gryn, K. and Tomsia, A.P. (2007), "Preparation of porous hydroxyapatite scaffolds", *Materials Science and Engineering: C*, Vol. 27 No. 3, pp. 546-550.

Şakar-Deliormanlı, A., Çelik, E. and Polat, M. (2008), "Rheological behavior of PMN gels for solid freeform fabrication", *Colloids and Surfaces A: Physicochemical and Engineering Aspects*, Vol. 324 Nos 1/3, pp. 159-166.

San Marchi, C., Kouzeli, M., Rao, R., Lewis, J.A. and Dunand, D.C. (2003), "Alumina-aluminum interpenetrating-phase composites with three-dimensional periodic architecture", *Scripta Materialia*, Vol. 49 No. 9, pp. 861-866.

Schlordt, T., Keppner, F., Travitzky, N. and Greil, P. (2012), "Robocasting of alumina lattice truss structures", *Journal of Ceramic Science and Technology*, Vol. 3 No. 2, pp. 81-88.

Schlordt, T., Schwanke, S., Keppner, F., Fey, T., Travitzky, N. and Greil, P. (2013), "Robocasting of alumina hollow filament lattice structures", *Journal of the European Ceramic Society*, Vol. 33 Nos 15/16, pp. 3243-3248.

Shonibare, O.Y. and Wardle, K.E. (2015), "Numerical investigation of vertical plunging jet using a hybrid multifluid–VOF multiphase CFD solver", *International Journal of Chemical Engineering*, Vol. 2015.

Smay, J.E., Cesarano, J. III and Lewis, J.A. (2002), "Colloidal inks for directed assembly of 3-D periodic structures", *Langmuir*, Vol. 18 No. 14, pp. 5429-5437.

Smay, J.E., Cesarano, J., Tuttle, B.A. and Lewis, J.A. (2004), "Directed colloidal assembly of linear and annular lead zirconate titanate arrays", *Journal of the American Ceramic Society*, Vol. 87 No. 2, pp. 293-295.

Stuecker, J.N., Cesarano Iii, J. and Hirschfeld, D.A. (2003), "Control of the viscous behavior of highly concentrated mullite suspensions for robocasting", *Journal of Materials Processing Technology*, Vol. 142 No. 2, pp. 318-325.

Travitzky, N., Bonet, A., Dermeik, B., Fey, T., Filbert-Demut, I., Schlier, L., Schlordt, T. and Greil, P. (2014), "Additive manufacturing of ceramic-based materials", *Advanced Engineering Materials*, Vol. 16 No. 6, pp. 729-754.

Vilčáková, J., Moučka, R., Svoboda, P., Ilčíková, M., Kazantseva, N., Hřibová, M., Mičušík, M. and Omastová, M. (2012), "Effect of surfactants and manufacturing methods on the electrical and thermal conductivity of carbon nanotube/silicone composites", *Molecules*, Vol. 17 No. 11, pp. 13157-13174.

Wang, J. and Shaw, L.L. (2005), "Rheological and extrusion behavior of dental porcelain slurries for rapid prototyping applications", *Materials Science and Engineering: A*, Vol. 397 Nos 1/2, pp. 314-321.

Wonisch, A., Polfer, P., Kraft, T., Dellert, A., Heunisch, A. and Roosen, A. (2011), "A comprehensive simulation scheme for tape casting: from flow behavior to anisotropy development", *Journal of the American Ceramic Society*, Vol. 94 No. 7, pp. 2053-2060.

Xie, B., Parkhill, R.L., Warren, W.L. and Smay, J.E. (2006), "Direct writing of three-dimensional polymer scaffolds using colloidal gels", *Advanced Functional Materials*, Vol. 16 No. 13, pp. 1685-1693.

Yalin, A., DeFoort, M., Willson, B., Matsuura, Y. and Miyagi, M. (2005), "Use of hollow-core fibers to deliver nanosecond Nd: YAG laser pulses to form sparks in gases", *Optics Letters*, Vol. 30 No. 16, pp. 2083-2085.

Yeo, A. and Fane, A. (2005), "Performance of individual fibers in a submerged hollow fiber bundle", *Water Science & Technology*, Vol. 51 Nos 6/7, pp. 165-172.

Corresponding authors

Zongwen Fu can be contacted at: zongwen.fu@fau.de and **Nahum Travitzky** can be contacted at: nahum.travitzky@fau.de

Downloaded by FRIEDRICH ALEXANDER UNIVERSITAET ERLANGEN NUERNBERG At 09:18 10 June 2018 (PT)

For instructions on how to order reprints of this article, please visit our website:
www.emeraldgrouppublishing.com/licensing/reprints.htm
Or contact us for further details: **permissions@emeraldinsight.com**